

Synthesis of metal sulfide nanomaterials *via* thermal decomposition of single-source precursors†

Ilan Jen-La Plante,^{ab} Tahani W. Zeid,^a Peidong Yang^{ab} and Taleb Mokari‡^{*bc}

Received 17th February 2010, Accepted 3rd June 2010

DOI: 10.1039/c0jm00439a

In this report, we present a synthetic method for the formation of cuprous sulfide (Cu₂S) and lead sulfide (PbS) nanomaterials directly on substrates from the thermolysis of single-source precursors. We find that the final morphology and arrangement of the nanomaterials may be controlled through the concentration of the dissolved precursors and choice of solvent. One-dimensional (1-D) morphologies may also be grown onto substrates with the addition of a metal catalyst layer through solution-liquid-solid (SLS) growth. These synthetic techniques may be expanded to other metal sulfide materials.

Introduction

Nanocrystal based solar cells have been demonstrated as a possible next generation lower-cost alternative to traditional silicon based solar cells.¹ Towards this end, the formation of inexpensive, earth-abundant nanomaterials for renewable energy is crucial to their potential utilization in large-scale solar cell applications.² One such material candidate is cuprous sulfide (Cu₂S), a naturally occurring abundant mineral with a bandgap of about 1.2 eV.³ Small variations in the electronic band structure arise depending on the crystal phase and stoichiometry. Based upon its elemental composition, Cu₂S offers a benign environmental profile when compared to its cadmium or lead based nanomaterial counterparts. This combination of properties positions Cu₂S as a leading material candidate for future solar applications.

Here, we present a simple synthetic method for the formation of cuprous sulfide (Cu₂S) nanocrystals *via* the thermal decomposition of a single-source molecular precursor, copper bisdiethyldithiocarbamate (Cu(II)[S₂CNC₄H₁₀]₂). This technique allows for large scale growth of the Cu₂S nanocrystals directly on a substrate. By changing the metal center in our single-source molecular precursor complex, we can grow a variety of metal sulfide nanomaterials including lead sulfide (PbS), cadmium sulfide (CdS), zinc sulfide (ZnS), and nickel sulfide (Ni₃S₂) among many other potential material combinations.

The precursor used in this synthesis, copper bisdiethyldithiocarbamate, is a volatile metal complex which exists primarily in

a dimeric crystalline form.⁴ The thermal decomposition of this molecule has been studied extensively by thermogravimetric analysis (TGA)⁵ and the reported decomposition range is from 200–300 °C with variances depending on the decomposition atmosphere (*i.e.* N₂, air, vacuum). Previous studies have determined a decomposition pathway based on gas chromatography (GC) and mass spectrometry (MS) measurements.⁵ A summary of this pathway is presented in Fig. 1A. Based on the GC/MS findings, it is reported that Cu(II)[S₂CNC₄H₁₀]₂ thermally

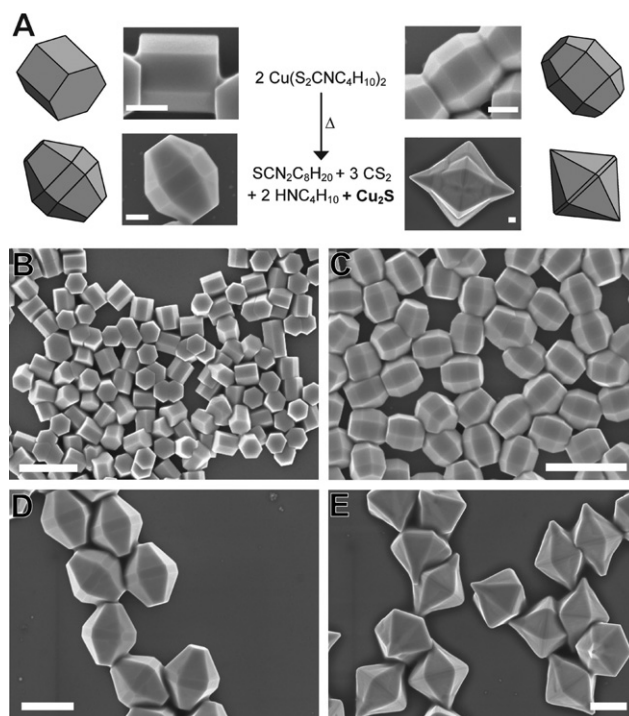


Fig. 1 Cuprous sulfide (Cu₂S) nanocrystals formed by thermally decomposing copper bis(diethyldithiocarbamate) (Cu[S₂CNC₄H₁₀]₂). A) Reported thermal decomposition pathway determined by mass spectrometry, scanning electron microscope (SEM) images and accompanying schematic drawings of different crystal shapes obtained (scale bars: 200 nm). B-E) Overview SEM images of crystal shapes shown in A) (scale bars: 1 μm).

^aDepartment of Chemistry, University of California Berkeley, Berkeley, CA, 94720, USA

^bMaterial Sciences Division, Lawrence Berkeley National Laboratory, Berkeley, CA, 94720, USA

^cThe Molecular Foundry, Lawrence Berkeley National Laboratory, Berkeley, CA, 94720, USA. E-mail: mokari@bgu.ac.il

† Electronic Supplementary Information (ESI) available: Supplementary information includes the formation of other metal sulfide nanomaterials on substrates, a comparison of the results of the thermolysis of the precursor in solution versus directly on substrate platforms, extended substrate areas following the SLS growth of Cu₂S and PbS 1-D morphologies, and X-ray diffraction pattern of Cu₂S nanowires. See DOI: 10.1039/c0jm00439a/

‡ Current address: Department of Chemistry and Ilse Katz Center for Nanoscience and Nanotechnology, Ben Gurion University of the Negev, Beersheva, Israel.

decomposes upon heating to form tetraethylthiourea ($\text{SCN}_2\text{C}_8\text{H}_{20}$), carbon disulfide (CS_2), and diethylamine ($\text{HNC}_4\text{H}_{10}$) which volatilize completely under heating; solid cuprous sulfide (Cu_2S) remains behind. The thermal decomposition of this molecule, $\text{Cu(II)[S}_2\text{CNC}_4\text{H}_{10}]_2$, to solid Cu_2S has been utilized in the formation of cuprous sulfide thin films *via* metal–organic chemical vapor deposition (MOCVD)⁶ or solution pyrolysis.⁷ Solution based decomposition of similar metal thiocarbamate molecules have also been shown to form nanoparticles, however, good control over size and morphology was not achieved.⁸ The use of single-source precursors in the solution-phase growth of nanowires has also been demonstrated as a way to solve the reactivity–balance problem. Recent work from the Buhro group has shown how the combination of solution-liquid-solid (SLS) mechanism reactions with single-source precursors can lead to the formation of PbS and CdS nanowires.⁹

Experimental details

All solvents and reagents were purchased from Sigma-Aldrich or Strem Chemicals and used as received. Scanning electron microscopy (SEM) was done using a Weiss Gemini Ultra-55 Analytical Scanning Electron Microscope operated at 5 kV. Transmission electron microscopy (TEM) was done using a JEOL 2100-F Field-Emission Analytical Transmission Electron Microscope operated at 200 kV. X-ray diffraction was performed on samples prepared on silicon substrates using a Bruker-AXS D8 with a general area detector and Cu $K\alpha$ radiation ($\lambda = 1.54 \text{ \AA}$). UV-vis absorbance measurements were made using a Shimadzu UV-3600.

Precursor synthesis

Single-source molecular precursors $\text{Cu(II)[S}_2\text{CNC}_4\text{H}_{10}]_2$ and $\text{Pb(II)[S}_2\text{CNC}_4\text{H}_{10}]_2$ were synthesized based on previously published methods.¹⁰ Briefly, Cu(II)Cl_2 , Pb(II)Cl_2 , and sodium diethyldithiocarbamate ($\text{Na(I)[S}_2\text{CNC}_4\text{H}_{10}]$) were dissolved separately in deionized water ($R > 18.0 \text{ M}\Omega$). The metal ion solution was mixed with the dissolved diethyldithiocarbamate ligand solution with a ligand to metal molar ratio of 2 : 1. The product formed immediately as a precipitate and was vacuum filtered and dried. The molecular precursor was recrystallized once from hot chloroform before use.

Cuprous sulfide synthesis

In a typical synthesis of the hexagonal nanoprisms, 6 μL of a 0.11 M solution of $\text{Cu(II)[S}_2\text{CNC}_4\text{H}_{10}]_2$ in trioctylphosphine (TOP 97%) is placed on a 6 mm \times 6 mm Si (100) substrate which has been cleaned by sonication in isopropanol. The substrate is placed onto a glass slide on a hot plate and heated under inert atmosphere (N_2) to $\sim 240\text{--}250 \text{ }^\circ\text{C}$ until all solvent has evaporated (about 10 min).

Lead sulfide synthesis

The synthesis is nearly unchanged from that of the cuprous sulfide, with the exception of the precursor solution

concentration. Here precursor concentrations used are 0.024, 0.048, 0.11, 0.195, and 0.22 M in TOP (Fig. 4A–E).

Nanowire synthesis

To form the Cu_2S and PbS nanowires on substrates, Si (100) substrates were first cleaned by sonication in isopropanol. Thermal evaporation was used to place a 2.0 nm sticking layer of chromium, followed by a 12.0 nm layer of bismuth. Upon heating the substrates, the Bi thin film melted forming molten droplets on the surface of the substrate, which act as catalysts in the formation of the solution-liquid-solid (SLS) grown nanowires. The amount of molecular precursor used per substrate area was increased for the nanowire syntheses to achieve a more suitable precursor to catalyst ratio. For the cuprous sulfide nanowires, 10 μL of a 0.44 M solution in TOP was used; for the lead sulfide nanowires, 15 μL of a 0.22 M solution was used. After adding the molecular precursor dissolved in TOP, the Bi covered substrates were heated to $\sim 250 \text{ }^\circ\text{C}$ and left at this temperature until all solvent had evaporated $\sim 10\text{--}14$ min.

Results and discussion

Copper bis(diethyldithiocarbamate) is decomposed in its dissolved form with trioctylphosphine as the solvent; final formation of the Cu_2S material occurs on silicon substrates. The dissolved precursor is placed onto a silicon substrate and heated to approximately $240\text{--}250 \text{ }^\circ\text{C}$ as determined by an IR thermometer. The decomposition reaction is allowed to proceed until all remaining organics have volatilized (about 10 min). The resulting Cu_2S nanostructures form in high yield, primarily as hexagonal nanoprisms as shown in the scanning electron microscope (SEM) image in Fig. 1B. Trioctylphosphine was chosen as an ideal solvent for its solubility of the molecular precursor, a boiling point that matches the decomposition temperature, and low vapor pressure.

When the synthesis is performed in higher vapor pressure solvents such as tributylphosphine or octadecene, the morphology of the Cu_2S nanoprisms remains unchanged; however, overall yield is markedly lower. Since changing the functional group or chain length of the solvent seems to have little effect on the shape of the nanostructures, we find that the primary role of the solvent is simply to provide a growth medium for the Cu_2S and prevent premature volatilization of the precursor. Additionally, the use of a low vapor pressure solvent and resulting slow evaporation rate allows for the neat arrangement and packing of the Cu_2S hexagonal disks. As can be seen in Fig. 2A–B, the hexagonal disks preferentially arrange with the hexagonal face touching the substrate surface. High packing densities can be achieved through this synthesis over large continuous areas of the substrate surface (Fig. 2B) with coverage as large as the surface area (36 mm^2) of the substrate used. Use of slow evaporation of a solvent to aid packing of nanostructures has been shown previously in the formation of aligned nanorod arrays¹¹ and the formation of nanoparticle superlattices.¹² This phenomenon of spontaneous orientation due to solvent drying is an important step towards the incorporation of these nanostructures to photovoltaic devices. The use of this synthetic method could obviate secondary assembly steps in Cu_2S

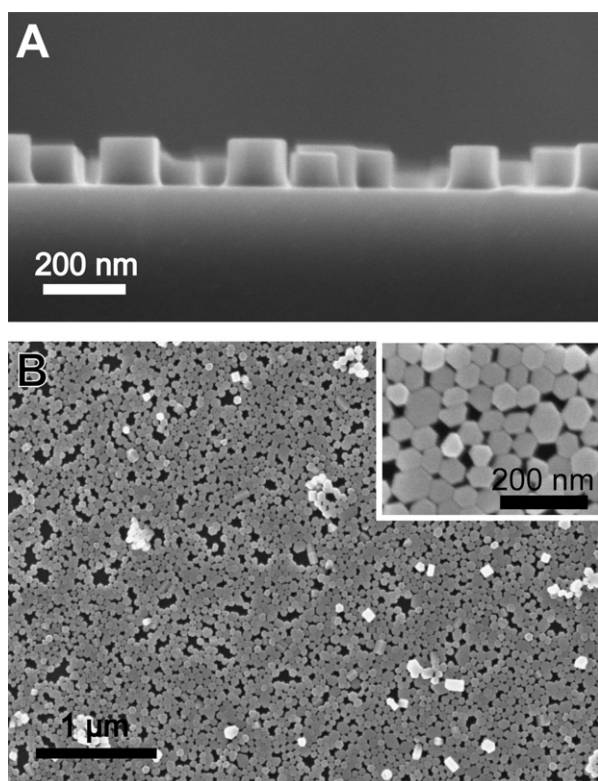


Fig. 2 Scanning electron microscope images of Cu_2S hexagonal nanodisks ordered on substrates. A) Cross-section view of low density coverage showing preferential orientation of the nanocrystals on the hexagonal faces. B) Top-down SEM view at low magnification showing higher packing density and continuity of coverage on the substrate, inset image is a higher magnification view of the same substrate.

nanocrystal-based photovoltaics. Currently, we are working to idealize the nanocrystal film and decrease vacancy concentrations.

When the reaction reaches completion, here defined by the complete evaporation of the trioctylphosphine, the average Cu_2S hexagonal nanoprism sizes are approximately 150–250 nm in diameter with an aspect ratio slightly higher than one (Fig. 1B). However, as shown in Fig. 2B, if the reaction is stopped by fast quenching in room-temperature toluene, smaller sizes of 50–100 nm may be achieved. A variety of other related nanostructures may also be formed from this type of reaction including hexagonal-cross section “nanokegs”, extended nanobarrels, and dodecahedron (Fig. 1C–E). These related structures form provided the solvent evaporation proceeds at a slow enough rate. Reactions performed in higher vapor pressure solvents, or those quenched in toluene before completion result only in the nanoprism morphology.

Since the nanocrystal nucleation is dependent on the original precursor concentration, this suggests that the main difference between the structures lies in the growth stage of formation. We suggest that the difference between formation of the nanoprisms, nanobarrels, extended nanobarrels, and dodecahedron is the local precursor concentration on the substrate during the growth stage. However, determining the exact concentration as the reaction progresses is non-trivial, due to competing factors of consumption of the precursor *via* nanocrystal formation with

a concentrating effect from the evaporation of the solvent. As a control, reactions with varying starting concentrations were performed in trioctylphosphine solution in a flask. At concentrations similar to those used in the growth of the nanoprisms on substrates (0.11 M), in the absence of any concentrating effect from solvent evaporation, nanocrystal growth stops as hexagonal plates with diameters slightly less than those of the substrate grown structures (Supporting Info Figure S1). When additional precursor material was injected to the reaction solution at a later time, the final aspect ratio of the hexagonal plates was higher, further confirming the need for additional precursor material to continue the growth along the top and bottom crystal faces.

All cuprous sulfide nanostructures show apparent six-fold rotational symmetry along the z -axis, a feature commonly reported in the monoclinic crystal phase of low-chalcocite.¹³ Twinning defects are the most commonly reported cause for this form of symmetry in the crystals;¹⁴ however, other explanations are possible. These include strain in the crystal lattice to accommodate the 120° angle required of a hexagonal structure. Another possibility stems from the high Cu ion mobility of chalcocite enabling rapid phase transformations between the high and low temperature stable forms of Cu_2S .¹⁵ For the Cu_2S system, three distinct crystal phases are possible including a low-temperature stable phase (monoclinic) stable below 104°C , a high-temperature stable phase (hexagonal), and a higher-T phase (tetragonal). Such ease of phase transition, due to the high cation mobility, may allow the Cu_2S hexagonal nanoprisms to form at 240°C in the high-T stable hexagonal crystal phase, but upon cooling to room temperature, experience rearrangements of the copper cation lattice to the low-T stable monoclinic crystal phase. Thus, the nanostructure could retain the bulk symmetry elements of a hexagonal nanoprism, while undergoing a rearrangement of the Cu cations. For both high-chalcocite (hexagonal) and low-chalcocite (monoclinic), the hexagonal close-packed sulfur anion lattice remains mainly unchanged between the two phases.^{13,15}

The Cu_2S nanoprisms were characterized by high-resolution transmission electron microscopy (HRTEM), X-ray diffraction (XRD), UV-vis absorbance (UV-vis) as shown in Fig. 3. From the HRTEM shown (Fig. 3A), taken from a top face of the nanoprism, we see that the Cu_2S nanoprisms have a high degree of crystallinity. The X-ray diffraction pattern for the cuprous sulfide hexagonal nanoprisms is shown in Fig. 3B. The XRD results indicate high phase-purity of the samples. All peaks present may be indexed to the low-temperature stable monoclinic crystal phase of Cu_2S (low-chalcocite, JCPDS 01-083-1462). Recent work from Korgel and coworkers¹⁶ as well as Alivisatos and coworkers¹⁷ report the synthesis of Cu_2S in the high-temperature stable hexagonal crystal phase. Other crystal phases of copper sulfide nanocrystals may also be produced through similar thermal decomposition techniques.¹⁸

Optical measurements were taken for the cuprous sulfide hexagonal nanoprisms. To perform a UV-vis absorbance measurement, a large area ($\sim 140\text{ mm}^2$) substrate covered with the as-made nanoprisms was sonicated briefly in toluene to suspend the material. The absorbance may be plotted as $(\alpha * E_{\text{hv}})^{1/2}$ versus E_{hv} , where α is the absorbance of the material and E_{hv} is the energy of the incident photon (Fig. 3C). We find a portion of this plot may be fitted linearly (circles) with an abscissa of $\sim 1.1\text{ eV}$ corresponding to a bandgap with the same value.

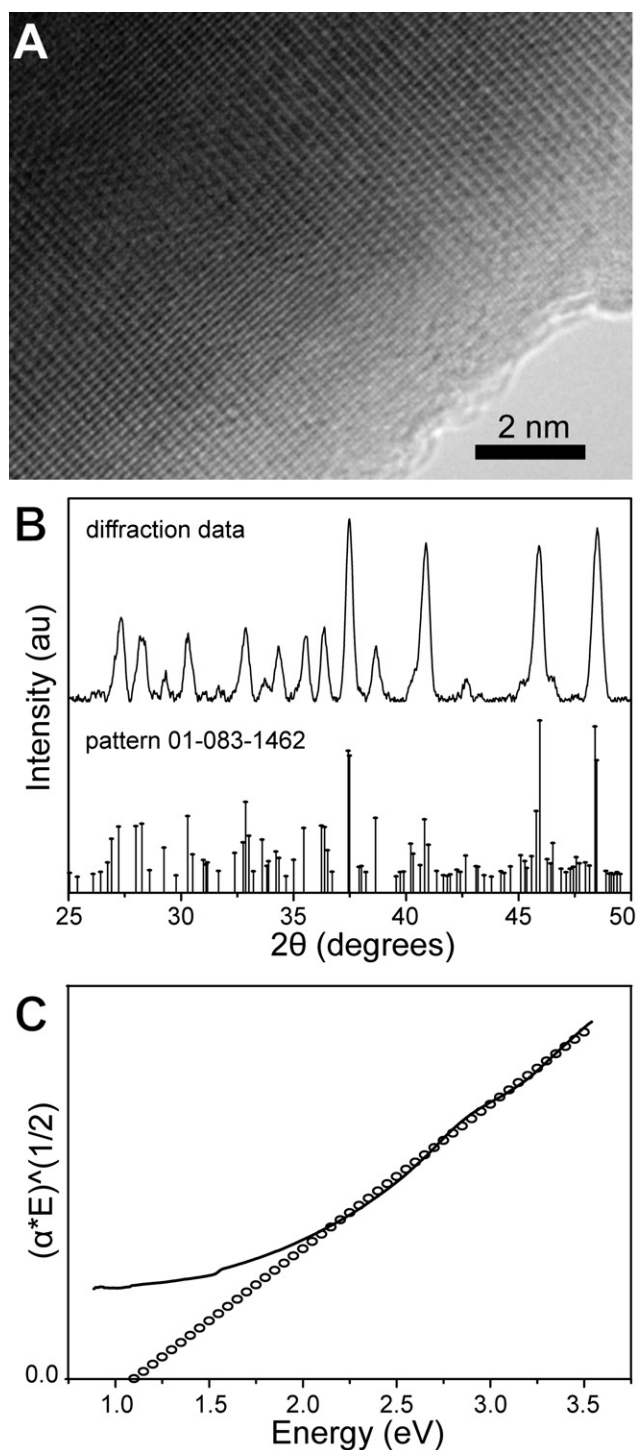


Fig. 3 A) High-resolution transmission electron microscopy (HRTEM) image of top face of Cu_2S hexagonal nanoprisms. B) Top trace shows X-ray diffraction pattern obtained from nanoprisms cast onto silicon substrates showing pure monoclinic phase Cu_2S (low-chalcocite). Droplines (shown below) correspond to data from published diffraction pattern JCPDS 01-083-1462. C) UV-vis absorbance is shown as a plot of $(\alpha \cdot E)^{1/2}$ versus E , where α is the sample absorbance and E is the incident wavelength energy.

To demonstrate the broader use of this synthetic technique in the formation of metal sulfides, a number of other metal bis(diethyldithiocarbamate)s including lead, cadmium, zinc, and

nickel, were synthesized and their decomposition products studied (Supporting Info Figure S2, S3). For the case of lead sulfide formation from $\text{Pb(II)[S}_2\text{CNC}_4\text{H}_{10}]_2$, we find a similar dependence of the nanocrystal morphology on concentration of the single-source molecular precursor in solution (Fig. 4). Thermal decomposition of $\text{Pb(II)[S}_2\text{CNC}_4\text{H}_{10}]_2$ was conducted at $\sim 250^\circ\text{C}$ at concentrations ranging from 0.024 M to 0.22 M in trioctylphosphine. For the lowest concentration, Fig. 4A, PbS nanostructures grow as rectangular sheets with additional growth on the sides and corners, reminiscent of a picture frame. Upon doubling, Fig. 4B, and quadrupling the concentration, Fig. 4C, the morphology changes to star-shapes structures and then branched star-shapes at 0.195 M (Fig. 4D). At the highest concentrations shown, Fig. 4E, all structures formed exhibit heavy branching. For the cubic crystal lattice of PbS, these six-armed star and branching dendritic morphologies are commonly reported for solution or hydrothermal syntheses.¹⁹

In these reactions, as the precursor concentration increases, two trends become clear. One is that higher concentrations yield larger structures and the other is that the level of branching seen in the crystals increases with concentration. These can both be explained by the additional molecular precursor material remaining in the growth stages at the higher concentrations, which may continue to grow additional material to the existing crystal structures. Here, no additional shape control agent or ligand is necessary to the formation of the various crystal

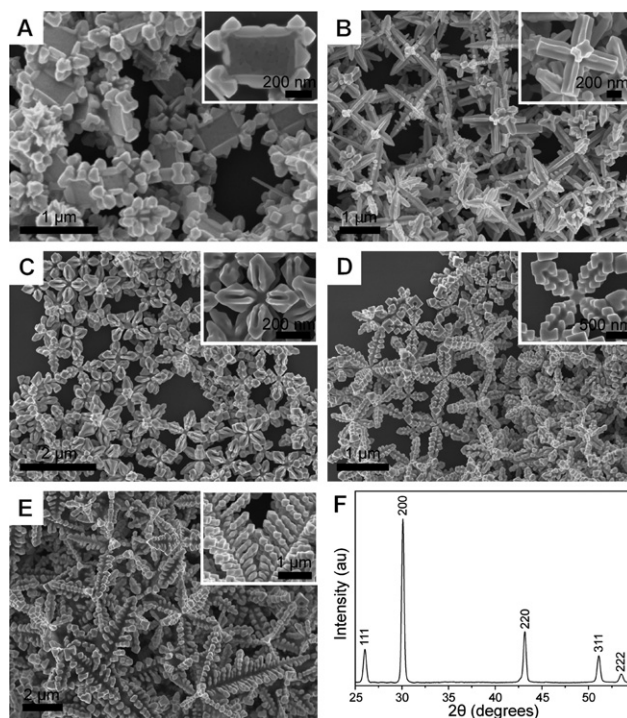


Fig. 4 Lead sulfide (PbS) formed by thermally decomposing lead bis(diethyldithiocarbamate) $\text{Pb(II)[S}_2\text{CNC}_4\text{H}_{10}]_2$. A-E) Different initial concentrations of molecular precursor in trioctylphosphine yield markedly different crystal growth morphologies. In sequence, the initial concentrations are 0.024, 0.048, 0.11, 0.195, and 0.22 M. F) X-ray diffraction pattern shows all peaks assigned to PbS crystal plane diffractions.

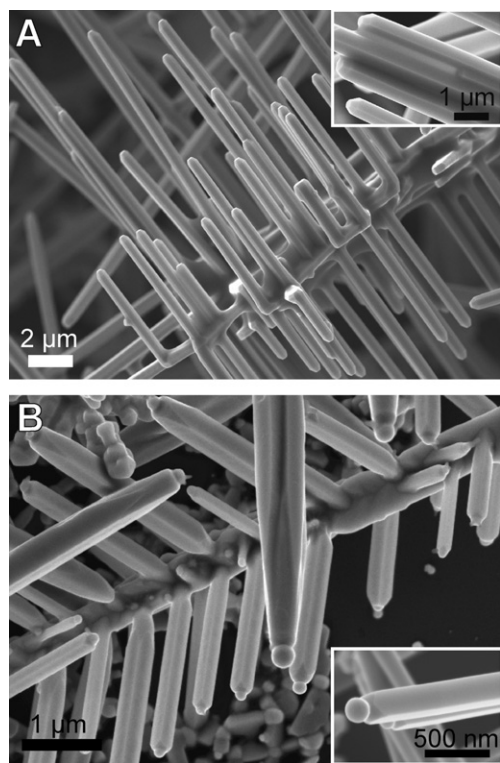


Fig. 5 Thermal decomposition of the $\text{Cu(II)[S}_2\text{CNC}_4\text{H}_{10}\text{]}_2$ and $\text{Pb(II)[S}_2\text{CNC}_4\text{H}_{10}\text{]}_2$ precursors in the presence of a catalyst yields branched wires *via* solution-liquid-solid (SLS) growth. A) Cu_2S (monoclinic) branched wires. B) PbS nanowires.

morphologies. X-ray diffraction (Fig. 4F) shows the materials to be crystalline PbS with all peaks indexed to the cubic crystal phase (Galena).

For solar cell applications, the structural morphology of nanomaterials has been shown to have great impact on the final device efficiency. Previous work comparing 0- and 1- dimensional systems in nanomaterial based solar cells has shown increased carrier mobility through a single-crystalline nanowire *versus* charge percolation through a nanoparticle thin film.²⁰ Thus, for nanowire based solar cells, the thickness of the inorganic layer may be engineered to maximize absorption based on absorption depth of the material with less effect on the carrier mobility.²¹ A number of methods have been developed for the growth of 1-D semiconductor nanowires in the solution phase, including ligand assisted anisotropic growth,²² oriented attachment,²³ solventless thermolysis,²⁴ and solution-liquid-solid (SLS).²⁵

Here, SLS mechanism catalyzed growth of nanowires is used to create an additional control over the resulting morphology from thermal decomposition of metal bis(diethylthiocarbamate)s on substrates. Use of SLS nanowire formation from a thermally evaporated catalyst layer has been demonstrated previously to form nanowires directly on substrates.²⁶ First we evaporate a chromium sticking layer (2 nm) followed by a bismuth catalyst thin film (12 nm) *via* thermal evaporation onto silicon substrates. Then thermal decomposition of either $\text{Cu(II)[S}_2\text{CNC}_4\text{H}_{10}\text{]}_2$ or $\text{Pb(II)[S}_2\text{CNC}_4\text{H}_{10}\text{]}_2$ in the presence of the melted Bi catalyst results in the 1-D growth of Cu_2S and PbS nanowires respectively

(Fig. 5, Supporting Info Figure S4). In order to achieve a high yield of nanowires, the ratio of molecular precursor to catalyst was optimized.

For both materials, concentrations used to form high nanowire yields were typically higher than those used for the growth of the non-catalyzed nanostructures. At the optimized concentrations, well-faceted nanowires with a high degree of branching are grown on the substrates. In the case of PbS, we observe the presence of a catalyst droplet at the tips of all nanowires (Fig. 5B), however, such spherical droplets were not observed on the Cu_2S . In previous work on SLS mechanism growth, the persistence or disappearance of a catalyst droplet has been shown to vary. For example, even within the same material system CdSe-Bi, Bi catalyst tips may or may not be found on the nanowire product depending on cooling conditions.²⁷ In our studies, at the precursor concentration used to form the Cu_2S *via* SLS, nanowires with 90° branched morphology do not form without the presence of a Bi thin film. This is strong evidence for the SLS mechanism in the formation of the Cu_2S branched structures, even without the presence of a catalyst droplet on the final product.

We note that for both materials, the branched arms occur with quasi-periodicity. This patterning phenomenon has been seen previously in studies on both metal film dewetting²⁸ and metal diffusion.²⁹ These observations – periodic branch spacing and the presence of catalyst tips – leads us to conclude that the branching likely occurs due to the mobility of the Bi droplets on the nanowire surfaces, resulting in the growth of further branching from the existing nanowires. Such branching growth mechanisms have been observed before in gas-phase synthesized PbS nanowire systems by Fardy *et al.*³⁰ as well as Yi and coworkers.³¹ Furthermore, we find that at lower precursor concentrations, nanowires exhibiting less branching and completely unbranched nanowires may be formed, due to the lack of additional precursor material to continue the branched nanowire growth. However, at these ratios of precursor to catalyst, the final chemical yield of nanowires is unsatisfactory. The crystal structures of the nanowire products were investigated by X-ray diffraction and were found to be the same as those of the nanocrystal products, that is, low-chalcocite Cu_2S and galena PbS (Supporting Info Figure S5).

Conclusions

In summary, we find that a variety of morphologies of metal sulfide nanomaterials may be grown from the simple thermal decomposition of a single-source molecular precursor in a compatible solvent system on substrates. The most important factor determining the final morphology appears to be the concentration of the single-source molecular precursor. For the case of cuprous sulfide (Cu_2S), nanostructures with six-fold symmetry are formed in the low-temperature stable monoclinic crystal phase (low-chalcocite). Spontaneous assembly of these structures when grown on substrates leads to close-packed monolayer formations which may be suitable for photovoltaic applications. For lead sulfide (PbS), the degree of branching observed in the nanocrystals formed increases with increasing precursor concentration. In both materials, SLS growth of 1-D nanowires on substrates is induced by the addition of a bismuth

catalyst thin film. In short, thermally decomposing metal sulfide single-source precursors in a moderate-boiling point solvent on substrates offers a simple method of creating a variety of semiconductor materials directly on substrates with control over structural morphology.

Acknowledgements

The authors wish to thank Dr. Shaul Aloni for assistance with transmission electron microscopy. Work at the Molecular Foundry was supported by the Director, Office of Science, Office of Basic Energy Sciences, Division of Materials Sciences and Engineering, U.S. Department of Energy, under Contract DE-AC02-05CH11231.

Notes and references

- I. Gur, N. A. Fromer, M. L. Geier and A. P. Alivisatos, *Science*, 2005, **310**, 462.
- C. Wadia, A. P. Alivisatos and D. M. Kammen, *Environ. Sci. Technol.*, 2009, **43**, 2072.
- B. J. Mulder, *Phys. Status Solidi A*, 1973, **15**, 409; B. J. Mulder, *Phys. Status Solidi A*, 1973, **18**, 633.
- M. Bonamico, G. Dessy, A. Mugnoli, A. Vaciago and L. Zambonelli, *Acta Crystallogr.*, 1965, **19**, 886.
- G. D'Ascenzo and W. W. Wendlandt, *J. Therm. Anal.*, 1969, **1**, 423; P. M. Madhusudanan, K. K. Mohammed Yusuff and C. G. Ramachandran Nair, *J. Therm. Anal.*, 1975, **8**, 31; C. G. Sceney, J. F. Smith, J. O. Hill and R. J. Magee, *J. Therm. Anal.*, 1976, **9**, 415.
- R. Nomura, K. Miyawaki, T. Toyosaki and H. Matsuda, *Chem. Vap. Deposition*, 1996, **2**, 174.
- R. Nomura, K. Kanaya and H. Matsuda, *Ind. Eng. Chem. Res.*, 1989, **28**, 877; S. Schneider, Y. Yang and T. J. Marks, *Chem. Mater.*, 2005, **17**, 4286; S. Schneider, A. Dzudza, G. Raudaschl-Sieber and T. J. Marks, *Chem. Mater.*, 2007, **19**, 2768; S. Schneider, J. R. Ireland, M. C. Hersam and T. J. Marks, *Chem. Mater.*, 2007, **19**, 2780.
- T. Trindale, P. O'Brien and X. Zhang, *Chem. Mater.*, 1997, **9**, 523; P. Yan, Y. Xie, Y. Qian and X. Liu, *Chem. Commun.*, 1999, 1293; T. Trindale, P. O'Brien, X. Zhang and M. Motevalli, *J. Mater. Chem.*, 1997, **7**, 1011.
- J. Sun and W. E. Buhro, *Angew. Chem. Int. Ed.*, 2008, **120**, 3259.
- O. F. Z. Khan and P. O'Brien, *Polyhedron*, 1991, **10**, 325.
- L. Li, J. Walda, L. Manna and A. P. Alivisatos, *Nano Lett.*, 2002, **2**, 557; J. L. Baker, A. Widmer-Cooper, M. F. Toney, P. L. Geissler and A. P. Alivisatos, *Nano Lett.*, 2010, **10**, 195.
- E. V. Shevchenko, D. V. Talapin, C. B. Murray and S. O'Brien, *J. Am. Chem. Soc.*, 2006, **128**, 3620.
- H. T. Evans, *Amer. Miner.*, 1981, **66**, 807; E. S. Dana, in *The system of mineralogy: descriptive mineralogy*, 5th Ed. (Eds: J. D. Dana, G. J. Brush), Wiley and son, New York, 1868, pp. 52.
- R. J. Cava, F. Reidinger and B. J. Wuensch, *Solid State Ionics*, 1981, **5**, 501.
- M. J. Buerger and B. J. Wuensch, *Science*, 1963, **141**, 276; H. T. Evans, *Science*, 1979, **203**, 356.
- T. H. Larsen, M. Sigman, A. Ghezelbash, R. C. Doty and B. A. Korgel, *J. Am. Chem. Soc.*, 2003, **125**, 5638; M. B. Sigman, Jr., A. Ghezelbash, T. Hanrath, A. E. Saunders, F. Lee and B. A. Korgel, *J. Am. Chem. Soc.*, 2003, **125**, 16050.
- Y. Wu, C. Wadia, W. Ma, B. Sadtler and A. P. Alivisatos, *Nano Lett.*, 2008, **8**, 2551.
- W. P. Lim, C. T. Wong, S. L. Ang, H. Y. Low and W. S. Chin, *Chem. Mater.*, 2006, **18**, 6170; W. Lou, M. Chen, X. Wang and W. Liu, *J. Phys. Chem. C*, 2007, **111**, 9658; Z. Zhuang, Q. Peng, B. Zhang and Y. Li, *J. Am. Chem. Soc.*, 2008, **130**, 10482; Y.-B. Chen, L. Chen and L.-M. Wu, *Chem.-Eur. J.*, 2008, **14**, 11069.
- Z. Quan, C. Li, X. Zhang, J. Yang, P. Yang, C. Zhang and J. Lin, *Cryst. Growth Des.*, 2008, **8**, 2384; G. Zhou, M. Lü, Z. Xiu, S. Wang, H. Zhang, Y. Zhou and S. Wang, *J. Phys. Chem. B*, 2006, **110**, 6543; M. S. Bakshi, P. Thakur, S. Sachar, G. Kaur, T. S. Banipal, F. Possmayer and N. O. Petersen, *J. Phys. Chem. C*, 2007, **111**, 18087.
- W. U. Huynh, J. J. Dittmer and A. P. Alivisatos, *Science*, 2002, **295**, 2425.
- M. Law, L. E. Greene, J. C. Johnson, R. Saykally and P. Yang, *Nat. Mater.*, 2005, **4**, 455.
- L. Manna, E. C. Scher and A. P. Alivisatos, *J. Am. Chem. Soc.*, 2000, **122**, 12700; L. Manna, E. C. Scher and A. P. Alivisatos, *J. Cluster Sci.*, 2002, **13**, 521.
- Z. Tang, N. A. Kotov and M. Giersig, *Science*, 2002, **297**, 237; C. Pacholski, A. Kornowski and H. Weller, *Angew. Chem., Int. Ed.*, 2002, **41**, 1188; K.-S. Cho, D. V. Talapin, W. Gaschler and C. B. Murray, *J. Am. Chem. Soc.*, 2005, **127**, 7140–7147.
- L. Chen, Y.-B. Chen and L.-M. Wu, *J. Am. Chem. Soc.*, 2004, **126**, 16334.
- T. J. Trentler, K. M. Hickman, S. C. Goel, A. M. Viano, P. C. Gibbons and W. E. Buhro, *Science*, 1995, **270**, 1791; F. Wang, A. Dong, J. Sun, R. Tang, H. Yu and W. E. Buhro, *Inorg. Chem.*, 2006, **45**, 7511–7521.
- L. Ouyang, K. N. Maher, C. L. Yu, J. McCarty and H. Park, *J. Am. Chem. Soc.*, 2007, **129**, 133; A. Dorn, C. R. Wong and M. G. Bawendi, *Adv. Mater.*, 2009, **21**, 3479; A. Dorn, P. M. Allen and M. G. Bawendi, *ACS Nano*, 2009, **3**, 3260; S. K. C. Lee, Y. Yu, O. Perez, S. Puscas, T. H. Kosel and M. Kuno, *Chem. Mater.*, 2010, **22**, 77.
- Z. Li, O. Kurtulus, N. Fu, Z. Wang, A. Kornowski, U. Pietsch and A. Mews, *Adv. Funct. Mater.*, 2009, **19**, 3650.
- P.-G. de Gennes, F. Brochard-Wyart, D. Quere, *Capillarity and Wetting Phenomenon*, (New York: Springer), 2003.
- R. D. Robinson, B. Sadtler, D. O. Demchenko, C. K. Erdonmez, L.-W. Wang and A. P. Alivisatos, *Science*, 2007, **317**, 355.
- M. Fardy, A. I. Hochbaum, J. Goldberger, M. M. Zhang and P. Yang, *Adv. Mater.*, 2007, **19**, 3047.
- J.-P. Ge, J. Wang, H.-X. Zhang, X. Wang, Q. Peng and Y.-D. Li, *Chem.-Eur. J.*, 2005, **11**, 1889.